Scaling Theory of Swelling and Deswelling of Polymer Networks

Tetsuya Yamamoto,[†,‡] Jonathan A. Campbell,[¶] Sergey Panyukov,[§] and Michael Rubinstein[*,†,‖]

†*Institute for Chemical Reaction Design and Discovery (WPI-ICReDD), Hokkaido University, Sapporo 001-0021, Japan.*

‡*PRESTO, Japan Science and Technology Agency (JST) - 4-1-8 Honcho, Kawaguchi, Saitama, 332-0012, Japan.*

¶*Department of Mathematics, Duke University, 120 Science Drive, Durham, NC 27708, United States.*

§*P. N. Lebedev Physics Institute, Russian Academy of Science, Moscow, Russia, 117924.*

‖*Departments of Mechanical Engineering and Materials Science, Biomedical Engineering, Physics, and Chemistry, Duke University, Durham, NC 27708, United States.*

E-mail: mr351@duke.edu

Abstract

We have developed a scaling theory of the elasticity of swollen and deswollen polymer networks. The elasticity of unentangled networks is primarily due to crosslinks, and the elasticity of entangled networks is due to trapped entanglements. In preparation conditions, the number of monomers N_{x} in strands of the unentangled network is less than the number of monomers N_{e0} in an entanglement strand while $N_{\mathrm{x}} > N_{\mathrm{e0}}$ for the entangled network. A network weakly entangled at preparation conditions is predicted to behave as unentangled network upon swelling. This "disentanglement" occurs due

to the separation of neighboring strands upon swelling, which reduces the restrictions on the fluctuations of strands due to their topological interactions with neighboring strands. A network unentangled at preparation conditions is predicted to behave as an entangled network upon deswelling if the number of overlapping network strands exceeds the Kavassalis-Noolandi number. The entanglements produced by network deswelling are transient and their number increases with deswelling, while the number of trapped entanglements is fixed by crosslinking. The "entanglement" upon deswelling and "disentanglement" upon swelling can be identified by measuring the concentration dependences of the elastic modulus.

1 Introduction

In this paper, we consider polymer networks obtained by random crosslinking or end-linking of an equilibrated semidilute polymer solution or melt.[1–3] In semidilute solutions in a good solvent, the sections of polymer chains with the number of monomers $n < g_0$ (g_0 is the number of monomers in the correlation volume) swell due to the excluded volume interactions between monomers of the same chain and are Gaussian for $n > g_0$, because these excluded volume interactions are screened by neighboring chains.[4,5] We consider cases where polymer chains are weakly crosslinked or end-linked, so that the average number $N_{\rm x}$ of Kuhn monomers of the network strands between crosslinks is greater than g_0. Under this assumption, the conformations of polymer chains are only slightly perturbed upon network formation. In the case of random crosslinking, the numbers of Kuhn monomers in network strands between neighboring crosslinks are distributed exponentially.[6]

The elasticity of polymer networks results from the suppression of fluctuations of polymer chains by crosslinks and entanglements.[3,4,7–9] The end-to-end vector $\mathbf{R}(n)$ of a chain section consisting of n monomers

$$\mathbf{R}(n) = \langle \mathbf{R}(n) \rangle + \delta \mathbf{R}(n) \tag{1}$$

is the sum of its time average $\langle \mathbf{R}(n) \rangle$ and the fluctuation size $\delta\mathbf{R}(n)$, defined as the instantaneous deviation of the vector $\mathbf{R}(n)$ from this average, see fig. 1**a**. Since the time average of the fluctuation size is zero, $\langle \delta\mathbf{R}(n) \rangle = 0$, the time-average of the square of the end-to-end distance of the segment can be written as the sum

$$\langle \mathbf{R}^2(n) \rangle = \langle \mathbf{R}(n) \rangle^2 + \langle \delta\mathbf{R}^2(n) \rangle. \tag{2}$$

Below, we use the simplified notation for the root-mean-square fluctuation size

$$\delta R(n) = \sqrt{\langle \delta\mathbf{R}^2(n) \rangle}. \tag{3}$$

The time-averaged square fluctuation size $\delta R^2(n)$ of sections of dangling chains in a network, as well as of chains in polymer liquids, monotonically increases with the number n of monomers up to the chain size, see the blue dotted line in fig. 1**b**. The time average of the end-to-end vectors of dangling chains is zero, $\langle \mathbf{R}(n) \rangle = 0$. These chains do not contribute to the elasticity of the network and are therefore called elastically ineffective. Chains are called elastically effective if their time-averaged end-to-end vectors $\langle \mathbf{R}(n) \rangle$ are non-zero. Short sections of elastically effective strands are only weakly affected by their connection to the network, and their mean square fluctuation size at preparation conditions $\delta R_0^2(n)$ is almost the same as in polymer liquids, see the green dashed line at $n < N_{\text{aff}0}$ in fig. 1. The subscript 0 indicates preparation conditions. In contrast, the fluctuation size $\delta R_0^2(n)$ of longer sections is suppressed by crosslinks and entanglements[1], compared to fluctuations of free or dangling chains, see the green dashed line at $n > N_{\text{aff}0}$ in fig. 1**b**. The crossover between these two regimes occurs at the affine strand $n = N_{\text{aff}0}$. The number of monomers N_{aff} in the affine strand is determined by specific assumptions of molecular models of polymer networks and is different in different models. It can be measured experimentally or by computer simulation

[1]For entangled networks, there is an intermediate regime, $\delta R(n) \sim n^{1/4}$, due to the longitudinal Rouse motion of strand sections along the tube, see fig. 1**b**.

by determining the number of monomers in the smallest linear section of a network that deforms affinely with (proportional to) the macroscopic deformation of the network. Upon network swelling, the number of monomers in the correlation volume and the number of monomers of the affine strand change from g_0 and $N_{\mathrm{aff}0}$ to g and N_{aff}, respectively (compare the green and magenta dashed lines in fig. 1**b**). Time-averaged end-to-end vectors of the elastically effective chain sections with $n > N_{\mathrm{aff}}$ monomers in the swollen network deform affinely with (proportionally to) the macroscopic deformation of the network (compare the green and magenta solid lines at $n > N_{\mathrm{aff}}$ in fig. 1**b**).

The shear modulus of a network can be written as the sum over all sections i containing N_{aff} Kuhn monomers in the network with volume V[4]

$$G(\phi) \approx \frac{k_{\mathrm{B}}T}{V} \sum_i \frac{\langle \mathbf{R}_i(N_{\mathrm{aff}})\rangle^2}{\langle \delta \mathbf{R}_i^2(N_{\mathrm{aff}})\rangle} \approx \frac{\phi}{v_b N_{\mathrm{aff}}} k_{\mathrm{B}}T \overline{\left[\frac{\langle \mathbf{R}(N_{\mathrm{aff}})\rangle^2}{\langle \delta \mathbf{R}^2(N_{\mathrm{aff}})\rangle}\right]}, \tag{4}$$

Eq. (4) is valid for networks that have a single length scale $R(N_{\mathrm{aff}})$, above which they deform affinely, such as networks prepared by crosslinking or endlinking precursor chains with the same molecular weight. Hereinafter, we use $\approx$ to denote the scaling equality up to a numerical constant of the order of unity. The average of a quantity A over all elastically effective strands in a network is denoted by $\overline{A}$. ϕ is the polymer volume fraction, v_b is the volume of a Kuhn monomer and, at the scaling level, it is on the order of b^3, the cube of the Kuhn length b.

For a weakly polydisperse network[2], the mean square fluctuation $\delta R^2(n)$ of section size does not significantly depend on the choice of the subsection. In such cases, the denominator in the square bracket in the last form of eq. (4) can be taken out of the average over elastically effective network sections. Then eq. (4) can be rewritten as

$$G(\phi) \approx k_{\mathrm{B}}T \frac{\phi}{N_{\mathrm{aff}} b^3} \frac{\mathcal{R}^2(N_{\mathrm{aff}})}{\delta R^2(N_{\mathrm{aff}})}, \tag{5}$$

[2]This refers to a network in which the distribution of the number of monomers of network strands is not multimodal.

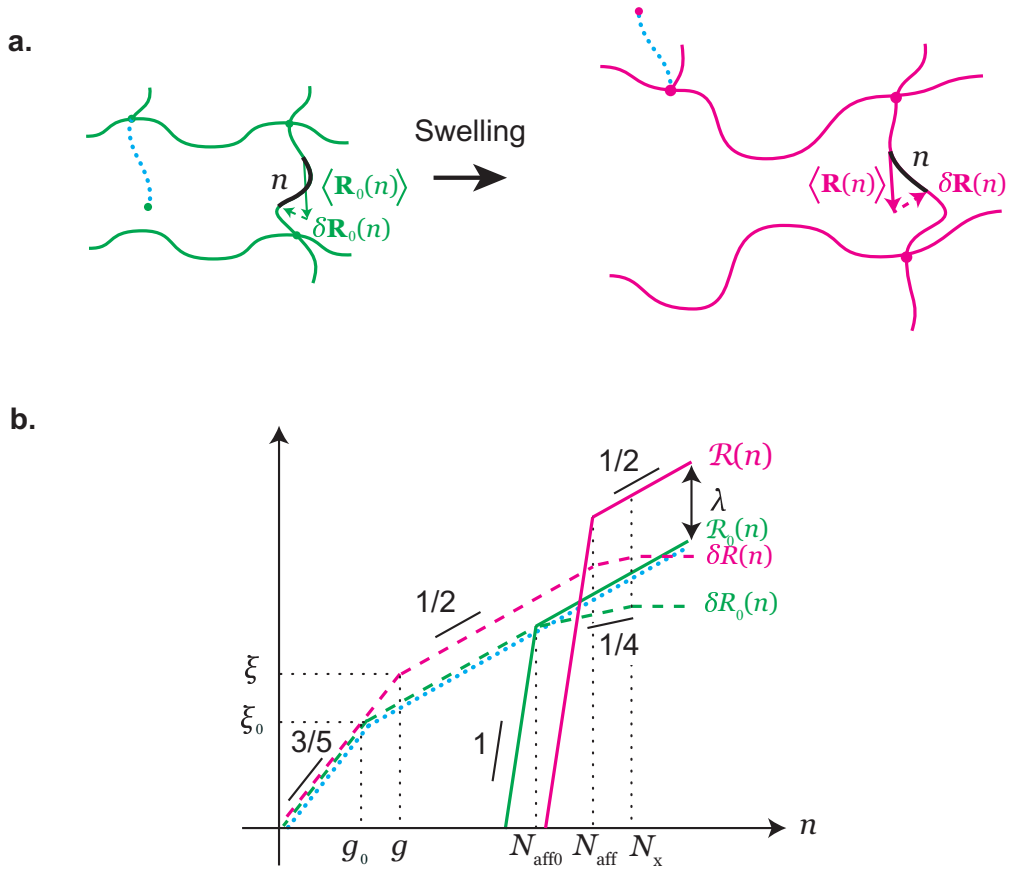

Figure 1: (**a**) Schematic representation of a polymer network at preparation conditions (left) and in the swollen state (right). The network was prepared and swollen in an athermal solvent. Dangling chains are shown by the blue dotted lines. (**b**) The root-mean-square fluctuation size $\delta R(n) \equiv \sqrt{\langle \delta \mathbf{R}^2(n) \rangle}$ of the end-to-end vector of a section of the dangling chain (blue dotted line) and of the elastically effective strand (dashed lines), as well as the RNST vector $\mathcal{R}(n) \equiv \sqrt{\overline{\langle \mathbf{R}(n) \rangle^2}}$ of the elastically effective strand (solid lines) as functions of the number of their monomers n. The quantities at the preparation conditions are indicated by the subscript 0 and shown by the green lines. The quantities in the swollen state are shown by the magenta lines. At preparation conditions, the correlation length is ξ_0 and the number of monomers in the correlation volume is g_0. In the swollen state, the correlation length is ξ and the number of monomers in the correlation volume is g. The number of monomers in the affine strand at the crossover between the constrained and unconstrained fluctuation regimes is $N_{\rm aff0}$ at the preparation conditions and $N_{\rm aff}$ in the swollen state. Both axes are logarithmic.

by using the simplified notation

$$\mathcal{R}(n) = \sqrt{\overline{\langle \mathbf{R}(n) \rangle^2}}. \tag{6}$$

We are introducing the acronym RNST end-to-end vector for $\mathcal{R}(n)$, the root of the network average of the square of the time-averaged end-to-end vector.

In the case of instantaneous crosslinking, the end-to-end vectors of chain sections composed of N_{aff} monomers are fixed by crosslinking at the magnitude of fluctuations in polymer solution (compare the blue dotted line and the green lines fig. 1**c**). The affine strand deforms affinely with the network deformation, $\mathcal{R}(N_{\mathrm{aff}}) \approx \lambda \mathcal{R}_0(N_{\mathrm{aff}})$, where λ is the linear extension ratio. In the cases of isotropic swelling or deswelling from preparation conditions with the polymer volume fraction ϕ_0 to the final volume fraction ϕ, the linear extension ratio λ is

$$\lambda = (\phi_0/\phi)^{1/3}. \tag{7}$$

The shear modulus of a homogeneous polymer network can thus be rewritten in the modified Panyukov form[10]

$$G(\phi) \approx \frac{\phi}{b^3 N_{\mathrm{aff}}} k_{\mathrm{B}} T \frac{\lambda^2 \mathcal{R}_0^2 (N_{\mathrm{aff}})}{\delta R^2 (N_{\mathrm{aff}})}. \tag{8}$$

The fluctuations of strands in the network are restricted both because of their connectivity to the rest of the network through crosslinks, and because of the topological interactions between neighboring strands due to the fact that these cannot pass through each other (the so-called *entanglements*). Networks are said to be unentangled if restrictions of fluctuations by the crosslinks are more important than the topological interactions. Otherwise, they are called entangled. There can be a wide crossover between these regimes, in which both crosslinks and entanglements make a significant contribution to network elasticity. Below we consider models for the limiting cases of unentangled ($N_{\mathrm{x}} \ll N_{\mathrm{e0}}$) and entangled ($N_{\mathrm{x}} \gg N_{\mathrm{e0}}$) networks. We then study cases in which N_{x} and N_{e0} are not very far from each other and,

by swelling or deswelling, one can crossover between unentangled and entangled network behaviors.

1.1 Models of unentangled polymer network

In the *affine network model*, the ends of network strands are fixed in space. It is instructive to consider that these ends are attached to a non-fluctuating background that deforms affinely with the network deformation, such as swelling.[1,3,4] Due to the randomness of the network connectivity, the positions of the attachment points of the ends of network strands to the non-fluctuating background are random variables, over which the network averaging is performed in eq. (4). The fluctuations of the ends of network strands are taken into account in the *phantom network model*.[2] The ends of the network strands in the phantom network model are constrained by crosslink potentials, which represent the confinement of the ends of network strands due to the elasticity of the rest of the network (blue strands in fig. 2**a**). The crosslink potentials can be represented by Gaussian *effective chains*. One end of the effective chain is connected to the end of the network strand, and the other end is attached to the non-fluctuating background. The effective chains do not contribute to the network stress. The number of monomers in the effective chain (light blue dashed lines in Fig. 2**b**) is proportional to the average number of monomers $N_{\rm x}$ in the network strand, with a coefficient depending on the functionality of crosslinks, and does not change upon network deformation. The number of monomers $N_{\rm aff}$ of affine strands thus scales proportionally to the number of monomers $N_{\rm x}$ of network strands.

1.2 Models of swollen entangled polymer networks

Topological interactions between network strands due to their non-crossability are taken into account in the tube models,[4,7,11] which represent these interactions by *topological potentials* that restrict the fluctuations of monomers of a network strand to a confining tube (fig. 2**c**). Topological potentials can be represented by Gaussian *virtual chains*, one end of which is

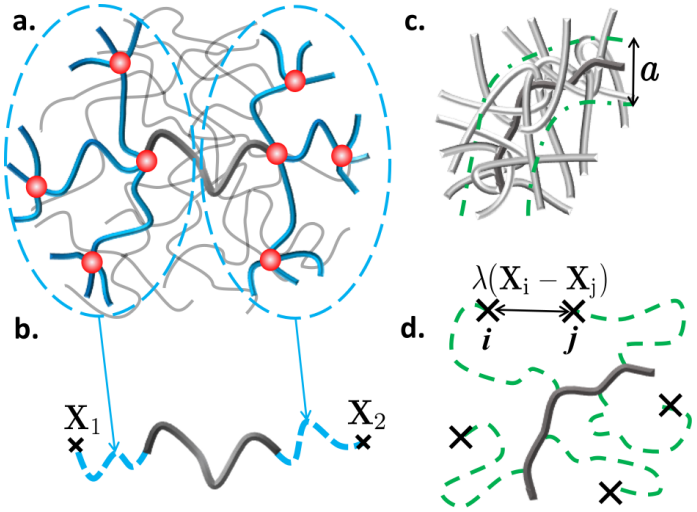

Figure 2: (a) In an unentangled network, the fluctuations of ends of network strands are suppressed due to their connection to neighboring strands. (b) In the phantom network model, the suppression of the fluctuations of network strands due to their connectivity to the rest of the network is represented by effective chains (light blue dashed lines). These effective chains connect crosslinks to the nonfluctuating background that deforms affinely with network deformation. (c) In an entangled network, the fluctuations of a network strand are confined by the tube (green dash-dotted lines) of diameter a due to the topological interactions between this strand and the surrounding strands. (d) The effective topological potentials acting on the network strand are represented by virtual chains (green dashed lines), which connect monomers of the strand to the non-fluctuating background. The attachment points (black "X"-s) of virtual chains to the non-fluctuating background are displaced affinely with the network deformation.

connected to the monomer of the network strand and the other end is attached to a point of the non-fluctuating elastic background (see green dashed lines in fig. 2**d**). Unlike ordinary potentials that are smoothly-varying functions of the monomer index, the topological potentials have minima at attachment points of virtual chains, which are randomly distributed in space.[12]

The simplest model of entangled polymer networks is the *affine tube model*.[4,7,11] It assumes that the stiffness of topological potential does not depend on the network deformation; therefore, the effect of the topological potential can be described by introducing additional crosslinks. In this model, the number of monomers N_{aff} in the affine strands scales proportionally to the number of monomers N_{e} of strands between adjacent entanglements, called entanglement strands, and it does not change with network deformation.[7]

More realistic models of entangled networks take into account the dependence of the topological interactions between entangled strands on their mutual overlap. With the network swelling, its strands move away from each other, which leads to a decrease in the stiffness of the topological potentials (and a corresponding increase in the number of monomers in virtual chains and in affine strands). In the non-affine tube model,[12–14] the dependence of the number of monomers of virtual chains on network deformation is determined by the self-consistency condition: since virtual chains were introduced only to represent the effect of topological interactions on conformations of network strands, they do not directly contribute to the elastic stress of the network.[12] The dependence of the number N_{aff} of monomers in affine strands on network deformation for various solvent conditions is discussed in Section 2 and Appendix A.

1.3 Models of deswollen entangled networks

Upon deswelling, the polymer volume fraction increases and network strands approach each other. Therefore, the stiffness of topological potentials increases with the network deswelling. The *non-affine tube model* assumes that strands remain Gaussian at all length scales from the

correlation length to the tube diameter.[12] With this assumption, the number of monomers in the entanglement strand decreases with an increase in the polymer volume fraction. Therefore, the non-affine tube model predicts that the number of effective entanglements increases upon network deswelling. However, the number of entanglements depends on network topology, which is fixed by crosslinking at network preparation conditions. In this paper, we propose an alternative model for deswelling of entangled networks that takes into account this constraint.

Fluctuations of network strands in a deswollen network are restricted by neighboring chains due to the non-crossability of polymer chains. Non-concatenated rings in a concentrated polymer solution experience analogous topological restriction if the concentration of the solution increases above the onset of entanglement while their non-concatenated ring topology remains fixed.[11] Such topological restrictions are called *transient entanglements* and are qualitatively different from entanglements in polymer solution of overlapping linear chains with Gaussian statistics conventionally described by tube models. In contrast to linear polymers, the equilibrium conformations of overlapping ring polymers are not ideal Gaussian. Originally, the lattice animal model was used to treat the transient entanglements in solutions and melts of entangled non-concatenated overlapping rings[15,16] as well as of deswollen networks.[11] More recently, it has been suggested that entangled non-concatenated rings form fractal loopy globules, in which the number of overlapping strand sections remains constant on all length scales exceeding the tube diameter of the solution of linear polymers at the same concentration ϕ.[17,18]

In this paper, we extend this description of transient entanglements between non-concatenated rings to the case of polymer networks and propose a new *non-affine loopy tube model* that takes into account the effects of crosslinks, trapped entanglements, and transient entanglements on the elasticity of swollen and deswollen polymer networks. The main predictions of our theory are

- Upon swelling, polymer networks that were entangled at preparation conditions expe-

rience weaker topological potential and, in some cases, could undergo a crossover to the unentangled regime (see $1 < N_{\rm x}/N_{\rm e0} < N_{\rm e}^{\rm eq}/N_{\rm e0}$ and the lower part of the magenta $\phi_{\rm e}/\phi_0$ line in fig. 3).

- Upon swelling, the shear modulus of entangled gels decreases with decreasing the polymer volume fraction ϕ stronger than expected by the affine tube model.

- Upon deswelling, the overlap of network strands increases, and transient entanglements are formed, even if network strands were unentangled at preparation conditions (see the upper part of the magenta $\phi_{\rm e}/\phi_0$ line in Fig. 3).

- Upon deswelling, the shear modulus of polymer gels in the regime of fractal loopy globule due to transient entanglements depends more strongly on polymer volume fraction ϕ than predicted by the phantom or affine tube model regardless of whether the network was entangled at preparation conditions or not.

In section 2, we discuss swelling and in section 3 deswelling of polymer networks prepared in athermal solvents. The results for other solvent conditions are summarized in Appendix A. We only consider cases where the solvent added to swell polymer networks is the same as in the conditions of network preparation. In section 4, we compare the predictions of our model with other models, experiments, and simulations. The physics of deswollen networks in a θ-solvent is described in Appendix B.

2 Swelling of polymer networks

2.1 Unentangled regime

Consider a polymer network prepared in an athermal solvent with a polymer volume fraction ϕ_0 higher than the overlap polymer volume fraction ϕ^*. If the number of (Kuhn) monomers $N_{\rm x}$ in a network strand is less than the number of monomers in the entanglement strand at

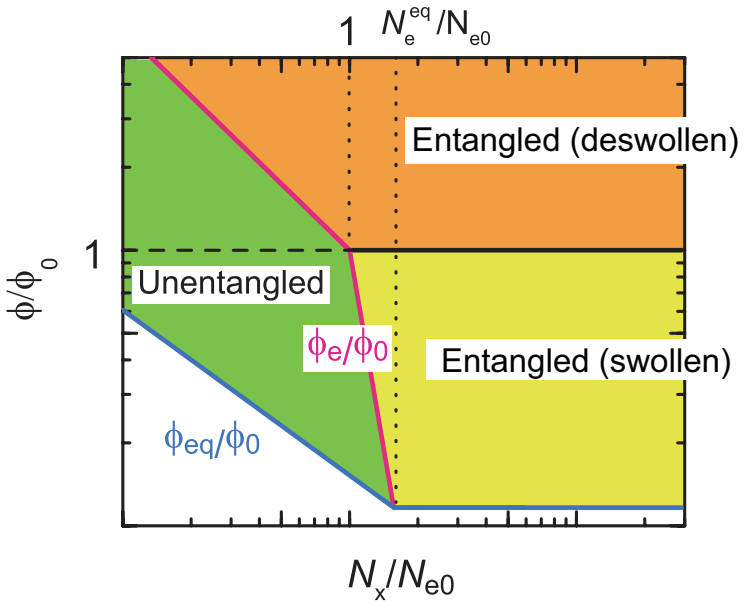

Figure 3: The diagram of regimes of polymer gels in an athermal solvent (double logarithmic plot). The vertical axis is the polymer volume fraction ϕ (rescaled by the polymer volume fraction ϕ_0 at preparation conditions) and the horizontal axis is the average number of monomers N_x in network strands (rescaled by the number N_{e0} of monomers in the entanglement strand at preparation conditions). Preparation conditions with $\phi/\phi_0 = 1$ are shown with a dashed horizontal line. The dotted vertical lines correspond to $N_x/N_{e0} = 1$ and $N_x/N_{e0} = N_e^{eq}/N_{e0}$. Polymer gels are swollen by adding athermal solvent ($\phi/\phi_0 < 1$) and are deswollen by removing this solvent ($\phi/\phi_0 > 1$). The polymer volume fraction ϕ_{eq} at the swelling equilibrium is shown by the cyan line. The crossover ϕ_e/ϕ_0 between entangled and unentangled regimes is shown by the magenta line. The shear modulus is determined by the contribution of crosslinks at $\phi < \phi_e$ (in the unentangled regime - green), and entanglements at $\phi > \phi_e$ (in the entangled regime). In the entangled regime, on length scales larger than the correlation length, the conformations of entanglement strands are Gaussian at $\phi < \phi_0$ (yellow) and fractal loopy globules at $\phi > \phi_0$ (brown). The crossover between the Gaussian regime and the fractal loopy globule regime is shown by the black horizontal line.

preparation conditions $N_{e0} \approx N_{em}\phi_0^{-5/4}$, the elasticity of the polymer network at preparation conditions is mainly due to the restrictions imposed by crosslinks. Here and below, we use the Flory exponent $\nu = 3/5$ to describe fluctuations of strand sections in an athermal solvent at small length scales[3].[4,5] At length scales smaller than the correlation length at preparation conditions $\xi_0 \approx b\phi_0^{-3/4}$, strand sections swell due to the excluded volume interactions between monomers of the same strand,[4,5] see the left section of the green dashed line in fig. 4. There are $g_0 \approx \phi_0^{-5/4}$ monomers in the correlation volume ξ_0^3. At length scales larger than ξ_0, the excluded volume interactions between monomers of the same strand are screened by the overlapping network strands, and these strands can be described as ideal chains of correlation blobs of size ξ_0,[4,5] see the right section of the green dashed line in fig. 4. The RNST end-to-end vector at preparation conditions is $\mathcal{R}_0(N_x) \approx b\phi_0^{-1/8}N_x^{1/2}$.

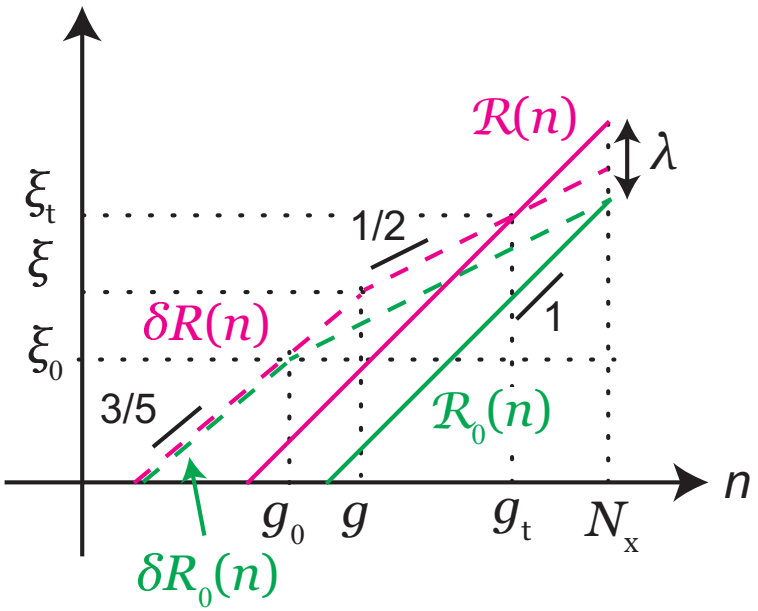

Figure 4: Dependence of the RNST end-to-end vector $\mathcal{R}(n)$, defined in eq. (6), (solid) and the root-mean-square fluctuation size $\delta R(n)$, defined in eq. (3), (dashed) of sections of network strands on their number of monomers n at preparation conditions (green) and in swollen unentangled gels (magenta). Axes are logarithmic.

With a decrease in the polymer volume fraction ϕ upon swelling, the correlation length increases, $\xi \approx b\phi^{-3/4}$. The correlation volume ξ^3 contains $g \approx \phi^{-5/4}$ monomers. Therefore,

[3]In Appendix A, we extend the calculation to other solvents and to a more accurate value of this exponent.

the fluctuation size of network strands increases to $\delta R(N_{\rm x}) \approx b\phi^{-1/8}N_{\rm x}^{1/2}$, which exceeds the size of network strands at preparation conditions by the factor of $\lambda^{3/8}$ $(= (\phi_0/\phi)^{1/8})$. The unentangled network strands deform affinely with the network deformation and, therefore, stretch upon swelling. The RNST end-to-end vector $\mathcal{R}(n)$ of the strand section is a linear function of its number of monomers n, (see the solid magenta line in fig. 4), while its fluctuation size increases as the square root of this number n at $n > g$ (see the right section of the magenta dashed line in fig. 4). The intersection of these two lines determines the size of the so-called tension blobs $\xi_{\rm t} \approx bN_{\rm x}^{1/2}\phi^{1/12}\phi_0^{-5/24}$, containing $g_{\rm t} \approx N_{\rm x}\lambda^{-5/4}$ monomers each. The shear modulus of the unentangled gel in athermal solvent has been derived by Panyukov[4,10] as

$$\begin{aligned} G(\phi) &\approx k_{\rm B}T\frac{\phi}{b^3N_{\rm x}}\frac{(\lambda\mathcal{R}_0(N_{\rm x}))^2}{\delta R^2(N_{\rm x})} \\ &\approx \frac{k_{\rm B}T}{N_{\rm x}b^3}\phi_0^{5/12}\phi^{7/12} \end{aligned} \tag{9}$$

see the green and light green lines at $\phi < \phi_0$ in fig. 5**b**. The shear modulus can also be represented as $k_{\rm B}T$ per tension blob, $k_{\rm B}T\phi/(b^3g_{\rm t})$.

The number of monomers in the affine strand of unentangled networks is proportional to the number $N_{\rm x}$ of monomers of network strands. As the polymer volume fraction decreases upon swelling, the correlation length ξ increases, whereas the size of the tension blob $\xi_{\rm t}$ decreases. The two characteristic lengths eventually become comparable $\xi_{\rm t} \approx \xi$ at the equilibrium swelling[19]

$$\phi_{\rm eq} \approx \phi_0^{1/4}N_{\rm x}^{-3/5}. \tag{10}$$

The equality of these length scales implies that the osmotic stress is balanced by the elastic stress in the network at the swelling equilibrium with the modulus $G_{\rm eq} \approx k_{\rm B}T/\xi_{\rm t}^3$.

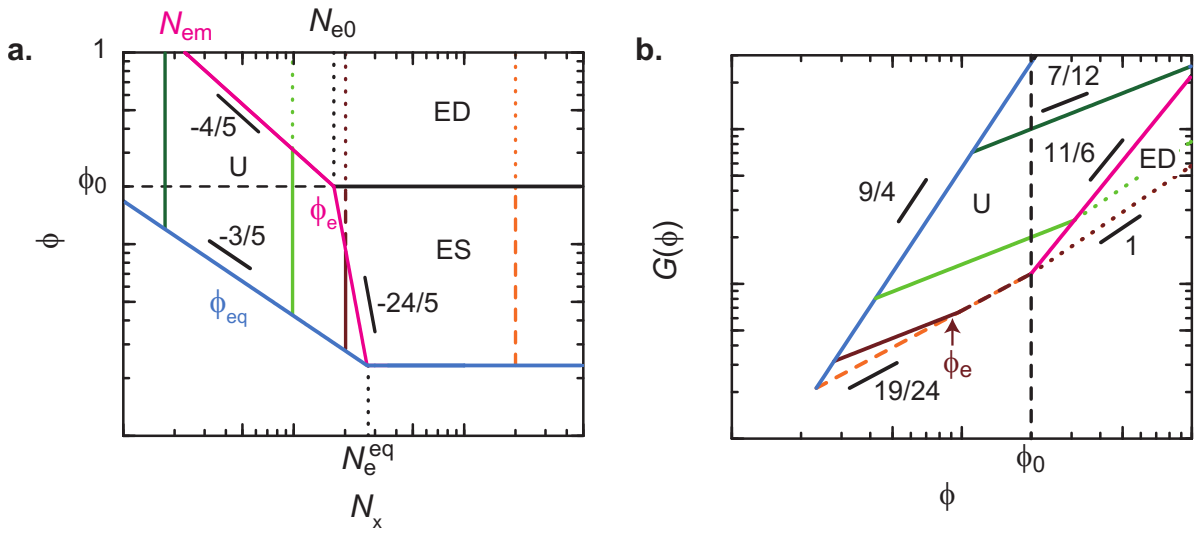

Figure 5: **a.** Diagram of regimes of polymer networks in an athermal solvent. The vertical axis is the polymer volume fraction ϕ and the horizontal axis is the number $N_{\rm x}$ of monomers in a network strand (double logarithm plot). The crossover line between the unentangled, 'U', and entangled swollen/deswollen regimes, 'ES' and 'ED', is shown by the magenta line. The crossover line between the entangled swollen, 'ES', and entangled deswollen 'ED' regimes is shown by the black solid line. The polymer volume fraction $\phi_{\rm eq}$ at equilibrium swelling is shown by the cyan line. **b.** The elastic modulus $G(\phi)$ of a polymer network crosslinked at the polymer volume fraction ϕ_0 (indicated by black vertical dotted line) as a function of the polymer volume fraction ϕ for several values of $N_{\rm x}$, shown by the vertical lines of the same color as in **a**, (double logarithmic plot). The elastic modulus at the unentangled-entangled crossover is indicated by the magenta line. The elastic modulus at the swelling equilibrium is indicated by the cyan line. The κ-exponents, defined by $G(\phi) \sim \phi^{\kappa}$, are 7/12, 19/24, and 1 in the unentangled (solid), entangled swollen (dashed), and entangled deswollen regimes (dotted), respectively. These lines are obtained by using the Flory exponent $\nu = 3/5$, see eqs. (9), (15), (21), and (23).

2.2 Entangled regime

The elasticity of the network at preparation conditions is dominated by the entanglements if the number N_x of monomers of network strands is greater than the number of monomers N_{e0} in entanglement strands at the preparation conditions. The conformations of the network strands at this volume fraction ϕ_0 are almost Gaussian on length scales larger than the correlation length ξ_0. The fluctuations of the network strands at preparation conditions are suppressed by the tube with diameter a_0 (see the green line for $n > N_{e0}$ in fig. 6). The RNST end-to-end vectors of the network strand sections are proportional to $n^{1/2}$ on length scales exceeding the tube diameter, because, on these scales, the chain sections can be described as a random walk with the primitive steps of size a_0 (see the second section of solid green line in fig. 6).

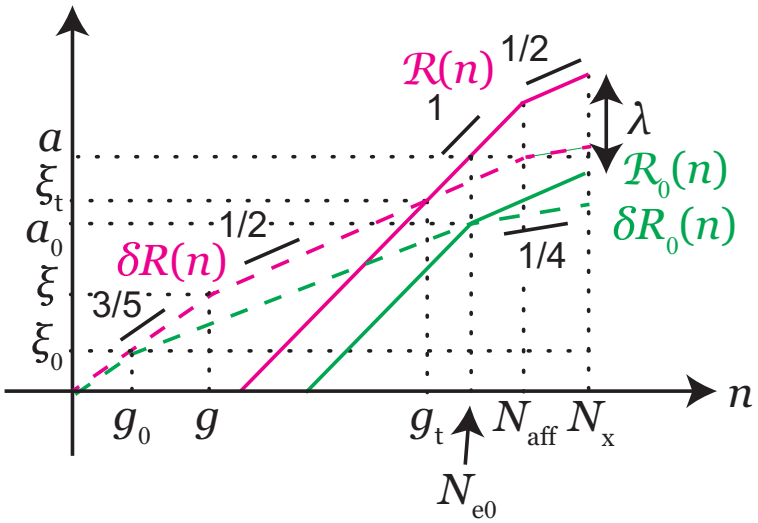

Figure 6: Dependence of the RNST end-to-end vector $\mathcal{R}(n)$ (solid lines) and root-mean-square fluctuation size $\delta R(n)$ (dashed lines) of the strand sections on the number n of their monomers in the entangled network at preparation conditions (green) and in the swollen state (magenta). Axes are logarithmic.

We will then extend the non-affine tube model[12] to describe the swelling of an entangled polymer network to the polymer volume fraction ϕ ($< \phi_0$). With a decrease in the polymer volume fraction, the correlation length ξ increases, and the entanglement strands swell. On length scales larger than the correlation length ξ, the root-mean-square fluctuation size $\delta R(n)$

of the strand section is proportional to the square root of the number of its monomers n, see the middle section of the dashed magenta line in fig. 6. At $n < N_{\rm aff}$, the RNST end-to-end vector $\mathcal{R}(n)$ of strand sections increases linearly with the number of monomers n in these sections, see the left part of the solid magenta line in fig. 6. The smallest sections of strand, the fluctuations of which are restricted to a tube of size

$$a \approx \delta R(N_{\rm aff}) \approx \xi \, (N_{\rm aff}/g)^{1/2} \, , \tag{11}$$

are affine strands, see the right end of the middle section of the dashed magenta line in fig. 6. The RNST end-to-end vector of longer sections, $n > N_{\rm aff}$, follows a primitive random walk path and deforms affinely, see the right section of the solid magenta line in fig. 6. The tube diameter is determined by the RNST end-to-end vector of the entanglement strand,

$$a \approx \mathcal{R}(N_{\rm e0}) \approx \lambda \mathcal{R}_0(N_{\rm aff}) \frac{N_{\rm e0}}{N_{\rm aff}}, \tag{12}$$

see the solid magenta line in fig. 6 at $n = N_{\rm e0}$. Here, $\mathcal{R}_0(N_{\rm aff}) \approx \xi_0 (N_{\rm aff}/g_0)^{1/2}$ is the RNST end-to-end vector of a strand subsection containing $N_{\rm aff}$ Kuhn monomers at the preparation conditions. By using the two expressions for the tube diameter, eqs. (11) and (12), the number of monomers $N_{\rm aff}$ of the affine strands is derived as

$$N_{\rm aff} \approx \lambda^{5/8} N_{\rm e0} \tag{13}$$

and the tube diameter is

$$a \approx \lambda^{11/16} a_0. \tag{14}$$

This implies that the tube diameter a does not change affinely with the linear extension ratio λ, but has a weaker dependence. The modified Panyukov expression, eq. (8), predicts that

the shear modulus of swollen entangled gels is

$$\begin{aligned} G(\phi) &\approx \frac{\phi}{b^3 N_{\rm aff}} k_{\rm B}T \frac{(\lambda \mathcal{R}_0(N_{\rm aff}))^2}{a^2} \\ &\approx \frac{k_{\rm B}T}{N_{\rm em} b^3} \phi_0^{35/24} \phi^{19/24}, \end{aligned} \tag{15}$$

see the orange dashed line at $\phi < \phi_0$ in fig. 5**b**, where $N_{\rm em}$ is the number of monomers of entanglement strands in the melt.

The intersection of the RNST end-to-end vector and the mean square fluctuation size gives the tension blob size $\xi_{\rm t} \approx \lambda^{1/16} a_0$, see the intersection of solid and dashed magenta lines in fig. 6. The number of monomers in the tension blob $g_{\rm t} \approx \lambda^{-5/8} N_{\rm e0}$ decreases upon network swelling. In contrast to unentangled networks (as well as entangled networks in θ-solvents), the size of tension blobs increases, albeit weakly, as the polymer volume fraction decreases upon swelling. This apparent anomaly results from an increase in $g_{\rm t}$ due to swelling ($\sim \phi^{-1/8}$), which is stronger than a decrease in $g_{\rm t}$ due to (swelling-induced) stretching ($\sim \phi^{5/48}$). The shear modulus can be also represented as $k_{\rm B}T$ per tension blob, $k_{\rm B}T\phi/(b^3 g_{\rm t})$, see eq. (15), as in the case of swollen unentangled networks, see also discussion below eq. (9).

The correlation length $\xi \approx b\phi^{-3/4}$ increases upon swelling with a larger negative exponent of the polymer volume fraction ($\sim \phi^{-3/4}$) than the tension blob size $\xi_{\rm t}$. The two length scales become comparable, $\xi(\phi) \approx \xi_{\rm t}$, at swelling equilibrium

$$\phi_{\rm eq} \approx \phi_0 N_{\rm em}^{-24/35}. \tag{16}$$

At swelling equilibrium, the osmotic pressure due to the excluded volume interactions between strands in the network is balanced by the elastic stress of the network[4]. In this case,

[4]Note that since the number of Kuhn monomers in the entanglement strand $N_{\rm em} \sim 30$, the maximum swelling is limited by entanglements to $\phi_0/\phi_{\rm eq} \sim N_{\rm em}^{24/35} \sim 10$ with the highest equilibrium linear expansion factor $\lambda_{\rm eq} \sim N_{\rm em}^{8/35} \sim 2$. Polyelectrolyte gels swell much more because counterions exert a much higher osmotic pressure.

the shear modulus is written as

$$G_{\rm eq} \approx \frac{k_{\rm B}T}{b^3} N_{\rm em}^{-54/35} \phi_0^{9/4}. \tag{17}$$

2.3 Disentanglement crossover upon swelling

There is an interval of the number of monomers of network strands, $N_{\rm e0} < N_{\rm x} < N_{\rm e}^{\rm eq}$, in which the networks that were entangled at preparation conditions change their elastic response upon swelling to that of unentangled gels (see the lower section of the magenta line in fig. 3). The crossover to unentangled regime occurs because upon swelling, the stiffness of the topological potentials, $k_{\rm B}T/a^2 \sim \phi^{11/24}$, decrease more steeply than the stiffness of the potentials due to crosslinks, $k_{\rm B}T/(\delta R^2(N_{\rm x})) \sim \phi^{1/4}$. With the degree of swelling corresponding to this crossover, the number of monomers $N_{\rm aff}$ in the affine strand becomes as large as the number of monomers $N_{\rm x}$ in the network strand, $\lambda_{\rm e} \approx (N_{\rm x}/N_{\rm e0})^{8/5}$, see eq. (13). The polymer volume fraction at the entangled-unentangled crossover upon swelling is

$$\phi_{\rm e} \approx \phi_0 \left(N_{\rm e0}/N_{\rm x}\right)^{24/5}, \tag{18}$$

as shown by the lower part of the magenta line in fig. 5**a**. Our present model thus predicts a change in the scaling exponent of the dependence of the shear modulus on the polymer volume fraction ϕ upon swelling from $19/24 \simeq 0.79$ in the entangled regime, $\phi_{\rm e} < \phi < \phi_0$, down to $7/12 \simeq 0.58$ in the unentangled regime, $\phi < \phi_{\rm e}$ at the disentanglement crossover, see the change in the slope of the brown line at $\phi_{\rm e}$ in fig. 5**b** and eqs. (9) and (15). There is a larger change of the dependence of the shear modulus on the volume fraction ϕ_0 at the preparation conditions at the disentanglement crossover from the scaling exponent $35/24 \simeq 1.46$ to $5/12 \simeq 0.42$, see the light green line in fig. 7**b** as well as eqs. (9) and (15).

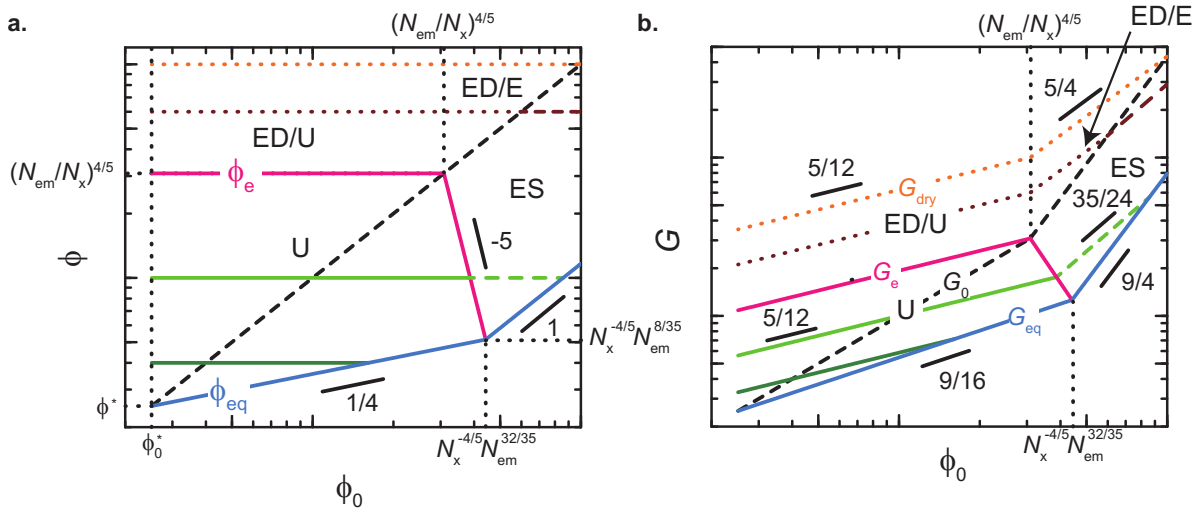

Figure 7: Diagram of regimes (**a**) and dependence of the elastic modulus G on the polymer volume fraction ϕ_0 at the preparation conditions (**b**) in an athermal solvent. The black dashed curve represents preparation conditions $\phi = \phi_0$. The crossover line between the unentangled ('U') regime and the entangled swollen/deswollen ('ES' and 'ED') regime is shown by the magenta line. The polymer volume fraction on the unentangled-entangled crossover at preparation conditions is $\phi_0 = (N_{\rm em}/N_{\rm x})^{4/5}$. The polymer volume fraction $\phi_{\rm eq}$ and the elastic modulus $G(\phi_{\rm eq})$ in the swelling equilibrium are shown by the cyan lines in **a** and **b**, respectively.

3 Deswelling of polymer gels

3.1 Unentangled regime ($N_{\rm x} < N_{\rm em}$)

If the number $N_{\rm x}$ of monomers in network strands is less than the number $N_{\rm em}$ of monomers of entanglement strands in the melt, the constraining effect of the crosslink potential on fluctuations of network strands prevails over the effect of the topological potential, see the region at $N_{\rm x} < N_{\rm em}$ in fig. 5**a**. In this case, the network is unentangled for all volume fraction ϕ, including the dry state, $\phi = 1$, regardless of the preparation concentration ϕ_0. The fluctuations of strands decrease with increasing polymer volume fraction due to a decrease in the correlation length ξ. The fluctuations of network strands are suppressed primarily by the crosslink potentials, see fig. 8**a**. The shear modulus of these networks with unentangled strands is thus given by eq. (9) for both swelling and deswelling, see the dark green curve in fig. 5**b**.

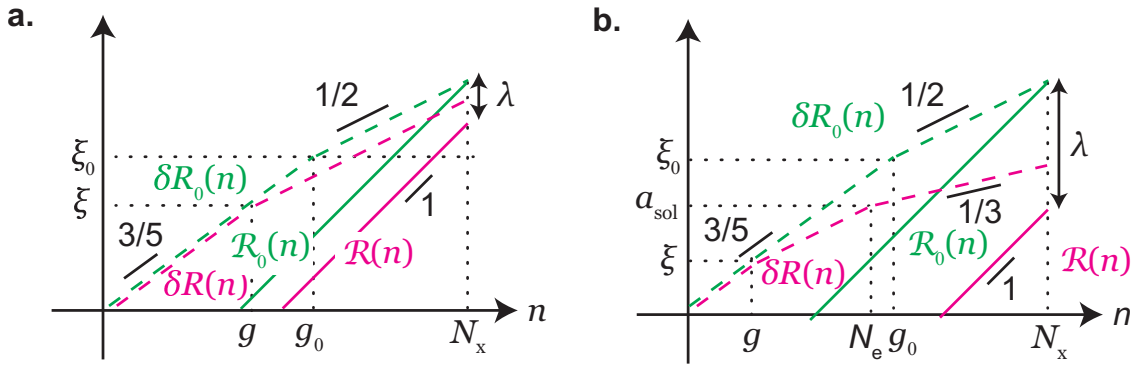

Figure 8: Dependence of the RNST end-to-end vector $\mathcal{R}(n)$ (solid lines) and the root-mean-square fluctuation size $\delta R(n)$ (dashed lines) of strand sections on the number n of their monomers in the deswollen network that was unentangled at preparation conditions and is in (**a**) the unentangled regime and (**b**) the entangled deswollen regime at **final conditions**. The green and magenta lines show the corresponding values at the preparation conditions and in the deswollen network. Axes are logarithmic.

3.2 Entangled regime ($N_{\mathrm{x}} > N_{\mathrm{e0}}$)

The networks were entangled at preparation conditions if the number of monomers N_{x} in the network strand is larger than the number of monomers N_{e0} in the entanglement strand at the preparation volume fraction ϕ_0. With increasing the polymer volume fraction upon network deswelling, neighboring strands approach to each other. The fluctuations of strand sections are suppressed due to the topological interactions with their neighboring strands, see fig. 9**a**. The topology of the network was fixed by crosslinking and thus the number N_{e0} of monomers per entanglement strands, which represents entanglements trapped at preparation conditions, remains constant. The situation, in which the concentration of overlapping chains increases at a fixed polymer topology is similar to the case of concentrated solutions of non-concatenated ring polymers. Unlike trapped entanglements of networks, the "entanglements" between rings are only transient and cannot transmit elastic stress. The fluctuations of rings in melts differ significantly from Gaussian fluctuations of linear polymer chains due to the presence of the transient entanglements.[17,18]

The Kavassalis-Noolandi criterion suggests that network sections composed of n monomers

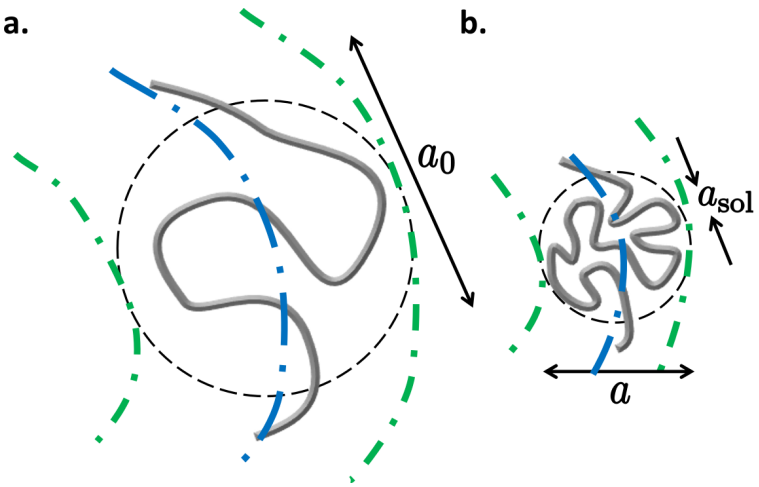

Figure 9: A chain section of a network is ideal in prepration conditions (**a**) and forms fractal loopy globules upon network deswelling (**b**). This is an example of a network that was entangled in preparation conditions and the fractuation of the chain section is confined by the tube of diameter a_0. Upon deswelling, the tube diameter changes to a. The chain section is still ideal for the length scales smaller than the tube diameter $a_{\rm sol}$ of a solution of the same concentration. The chain section form a fractal loopy globule in the length scales between $a_{\rm sol}$ and a.

are entangled if the overlap parameter of these sections[5]

$$\mathcal{O}(n) = \frac{\phi \delta R^3(n)}{b^3 n}. \tag{19}$$

is larger than the number $N_{\rm em}^{1/2}$.[20,21] According to this criterion, transient entanglements are not significant for strand sections composed of n monomers at $n < N_{\rm e}(\phi)$ ($\approx N_{\rm em}\phi^{-5/4}$). On length scales smaller than the smallest length scale $a_{\rm sol}(\phi)$ of transient entanglements, strand sections consisting of n monomers thus swell at $n < g$ and are Gaussian at $g < n < N_{\rm e}(\phi)$ (see the two left sections of dashed magenta line in fig. 10), as in the case of unentangled networks, see sec. 3.1. Transient entanglements are only significant at $n > N_{\rm e}(\phi)$ (at the volume fraction $\phi > \phi_0$). The fractal loopy globule model predicts that the fluctuation size

[5]For network strands composed of non-spherical Kuhn monomers, the overlap parameter is generalized to

$$\mathcal{O}(n) = \frac{\phi \delta R^3(n)}{v_b n}.$$

The Kavassalis-Noolandi number is $b^3 N_{\rm em}^{1/2}/v_b$.

of transiently entangled strand sections is determined from the condition of the saturation of the overlap parameter $\mathcal{O}(n)$ at $n > N_{\rm e}(\phi)$.[17,18] The last condition describes fluctuations of fractal loopy globules on length scales $a_{\rm sol} < \delta R(n) < a$

$$\delta R(n) \approx a_{\rm sol}\,(n/N_{\rm e})^{1/3}\,, \tag{20}$$

where $a_{\rm sol}$ $(= a_{\rm em}\phi^{-3/4})$ is the tube diameter of polymer solution of the same volume fraction ϕ (with the tube diameter in melts, $a_{\rm em} = bN_{\rm em}^{1/2}$).

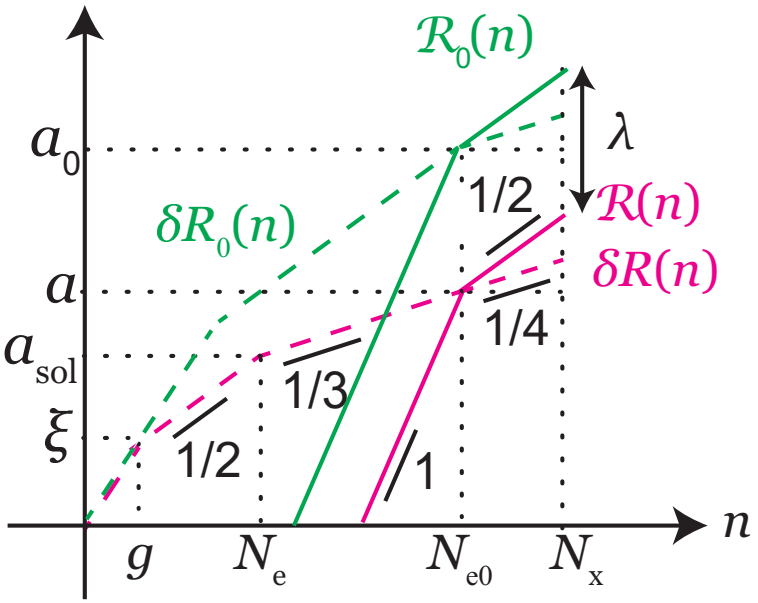

Figure 10: Dependence of RNST end-to-end vector (solid lines) and root-mean-square fluctuation size (dashed lines) of strand sections in deswollen networks that were entangled at preparation conditions on the number n of their monomers. The quantities at preparation conditions and for the deswollen networks are shown by the green and magenta lines, respectively. Axes are logarithmic.

Sections of network strands composed of n monomers form fractal loopy globules at $N_{\rm e} < n < N_{\rm e0}$, see the third section of the magenta dashed line with slope 1/3 in fig. 10. Fluctuations of strand sections with $n > N_{\rm e0}$ occurs along the confining tube (breathing modes) with $\delta R(n) \sim n^{1/4}$, see the fourth section of the magenta dashed line at $n > N_{\rm e0}$ in fig. 10. The number of monomers $N_{\rm aff}$ in the affine strand of deswollen entangled networks $N_{\rm e0}$ does not depend on the degree of deswelling. The tube diameter is thus $a \approx \lambda a_0$ and it

changes affinely with the network deswelling, [6] compare the right parts of green and magenta dashed lines in fig. 10.

The RNST end-to-end vector of chain sections increases linearly with the number n of monomers of this section, if it is shorter than the length of the trapped entanglement strand, $n < N_{e0}$, and increases proportionally to the square root of n for $n > N_{e0}$ (see the solid green and red lines in fig. 10). For $n > N_{e0}$, the RNST end-to-end vector of the sections changes affinely with the network deswelling. Thus, the shear modulus of the deswollen entangled network increases linearly with the polymer volume fraction

$$\begin{aligned} G(\phi) &\approx k_B T \frac{\phi}{N_{e0} b^3} \frac{(\lambda \mathcal{R}_0(N_{e0}))^2}{a^2} \\ &\approx \frac{k_B T}{b^3 N_{em}} \phi_0^{5/4} \phi, \end{aligned} \tag{21}$$

see the right dotted section of the brown line at $\phi > \phi_0$ in fig. 5**b**. The RNST end-to-end vector of the entanglement strand at the preparation conditions is equal to its fluctuation size, $\mathcal{R}_0(N_{e0}) = b\phi_0^{-1/8} N_{e0}^{1/2}$ (see intersection of green solid and dashed lines in fig. 9). The overlap parameter of network strands is equal to the Kavassalis-Noolandi number, $N_{em}^{1/2}$, already at preparation conditions. Therefore, at $\phi > \phi_0$, the entanglement strands form fractal loopy globules, see figs. 3 and 9. The window of length scales from a_{sol} to a, for which strand sections form fractal loopy globules, enlarges with increasing polymer volume fraction ϕ.

3.3 Entanglement crossover upon deswelling

Consider the case when the number of monomers N_x in the network strand is smaller than the number of monomers N_{e0} in the entanglement strand under preparation conditions, but larger than the number of monomers N_{em} in an entanglement strand in the melt, $N_{em} < N_x < N_{e0}$. The width of this interval scales as $N_{e0}/N_{em} \approx \phi_0^{-5/4}$ and is larger than the width of the

[6] It is not the case for networks deswollen in θ-solvents (see Appendix A).

disentanglement interval $N_{\rm e}^{\rm eq}/N_{\rm e0} \approx N_{\rm em}^{1/7}$ for $\phi_0 < N_{\rm em}^{-4/35}$. At preparation conditions, the overlap parameter of network strands is smaller than the Kavassalis-Noolandi number $N_{\rm em}^{1/2}$ and the network is thus unentangled. The overlap parameter increases with increasing polymer volume fraction ϕ upon deswelling as $\mathcal{O}(N_{\rm x}) \approx \phi \delta R^3(N_{\rm x})/(b^3 N_{\rm x}) \approx \phi^{5/8} N_{\rm x}^{1/2}$, where the fluctuations of the network strand are $\delta R(N_{\rm x}) \approx b\phi^{-1/8} N_{\rm x}^{1/2}$. As long as the number of overlapping network strands is lower than the Kavassalis-Noolandi number $N_{\rm em}^{1/2}$, the fluctuations of network strands with the number n of monomers, $g < n < N_{\rm x}$, are Gaussian, see the right section of the magenta dashed line in fig. 8**a**. The network is thus unentangled in this regime and its shear modulus is given by eq. (9).

If the number of overlapping network strands reaches the Kavassalis-Noolandi number $N_{\rm em}^{1/2}$, these strands form fractal loopy globules on length scales larger than the tube diameter $a_{\rm sol}$ of a polymer solution with the same volume fraction ϕ. The polymer volume fraction at the crossover between the unentangled and entangled regimes, determined by the condition, $\mathcal{O}(N_{\rm x}) \approx \phi_{\rm e}^{5/8} N_{\rm x}^{1/2} \approx N_{\rm em}^{1/2}$, is

$$\phi_{\rm e} = (N_{\rm em}/N_{\rm x})^{4/5} \tag{22}$$

as shown by the upper part of the magenta line in fig. 5**a**. The sections of network strands are unentangled at $n < N_{\rm e}$ (the second part of the magenta dashed line in fig. 8**b**) and form fractal loopy globules at $N_{\rm e} < n < N_{\rm x}$ (the third part of the magenta dashed line in fig. 8**b**).

Because, in the latter regime, the fluctuations of network strands are $\delta R(N_{\rm x}) \approx a_{\rm sol}(N_{\rm x}/N_{\rm e})^{1/3}$, see eq. (20), the shear modulus of deswollen networks varies linearly with the volume fraction of the gel

$$G(\phi) \approx \frac{k_{\rm B}T}{N_{\rm x}^{2/3} N_{\rm em}^{1/3} b^3} \phi_0^{5/12} \phi, \tag{23}$$

see the light dotted green line of fig. 5**b**. Note that whether networks were entangled or unentangled in preparation conditions results in the significant difference in the scaling

exponents $5/4 = 1.25$ and $5/12 \simeq 0.42$ that describe the dependence of the shear modulus on the polymer volume fraction in the preparation conditions ϕ_0 in the entangled deswollen regime, see the orange and brown dotted lines in fig. **7b** and also eqs. (21) and (23). This difference reflects the strong dependence of the tube diameter on ϕ_0 under entangled preparation conditions.

The fluctuations $\delta R(N_{\rm x})$ of network sections are suppressed by transient entanglements in the entangled deswollen regime, and network strands are Gaussian on length scales larger than correlation length in the unentangled regime. The fluctuations $\delta R(N_{\rm x})$ of network strands do not depend on the polymer volume fraction ϕ_0 at preparation conditions because they are determined only by the number of overlapping strands at the final condition, see eq. (19). The dependence of the elastic modulus on ϕ_0 in the entangled deswollen regime, eq. (23), is therefore the same as that in the unentangled regime, see eq. (9) and fig. **7b**.

4 Discussion

There are three regimes of polymer network elasticity: the unentangled (U), entangled swollen (ES), and entangled deswollen (ED) regimes, see figs. 5 and 7, with different scaling exponents κ_0 and κ that represent the dependence of network shear modulus, $G \sim \phi_0^{\kappa_0}\phi^{\kappa}$, on the volume fractions ϕ_0 at preparation conditions and ϕ at final conditions. The non-affine loopy tube model predicts the disentanglement crossover, in which networks that were entangled at preparation conditions ($N_{\rm e0} < N_{\rm x}$) become unentangled upon network swelling if $N_{\rm x} < N_{\rm e}^{\rm eq}$. It also predicts the entanglement crossover, in which networks that were unentangled at preparation conditions ($N_{\rm x} < N_{\rm e0}$) become entangled upon network deswelling if $N_{\rm x} > N_{\rm em}$. There are four scenarios of crossovers between different regimes by changing the polymer volume fraction ϕ of the polymer network, see dark green, light green, brown, and orange lines in fig. **5a**. There are three crossover scenarios by changing the polymer volume fraction ϕ_0 at the preparation conditions of polymer networks; see dark green, light

green, and brown lines in fig. 7**a**. The predictions of this model can be tested experimentally (or via simulations) by detecting the disentanglement and entanglement crossovers and by measuring the scaling exponents in each of the corresponding regimes.

4.1 Entanglement crossover

The entanglement crossover upon deswelling was detected by experiments and simulations on end-linked networks of tetra-PEG.[22–24] The simulation results by Asai *et al.*[24] are in good agreements with the function

$$\frac{G(\phi)}{G(\phi_0)} = \left(\frac{\phi}{\phi_0}\right)^{0.56} \left[1 + \left(\frac{\phi}{\phi_\mathrm{e}}\right)^{0.44k}\right]^{1/k}, \tag{24}$$

describing the crossover between the unentangled gel regime (U - eq. (9)) and the entangled deswollen regime (ED - eq. (23)), see fig. 11**b**. The polymer volume fraction at the entanglement crossover is estimated to be $\phi_\mathrm{e} = 0.46$ by fitting eq. (24) to the simulation data.[24] This estimate is close to the value $\phi_\mathrm{e} \approx 0.4$ obtained by using eq. (S22') in the Supporting Information with $N_\mathrm{x} = 100$ and $N_\mathrm{em} = 30$. The fitting parameter k is estimated to be 5.0, implying that the crossover is rather sharp. The entanglement crossover can be detected experimentally upon deswelling polymer networks from the preparation conditions between polymer overlap and entanglement folume fractions $\phi^* < \phi_0 < \phi_{\mathrm{e}0}$ up to the dry state, $\phi = 1$, as long as one uses polymers that do not crystallize or become glassy in the dry state.

Katashima and coworkers measured the dependence of the elastic modulus $G(\phi)$ of tetra-PEG in an ionic liquid, 1-butyl-3-methylimidazolium tetrafluoroborate, on the polymer volume fraction ϕ. This experiment revealed that the exponent κ that represents the dependence of $G(\phi)$ on ϕ increases from ≈ 0.56 upon small deswelling to approximately unity for stronger deswelling, which is consistent with our prediction of the entanglement crossover, see sec. S4.1 and Figure S4 in the Supporting Information.

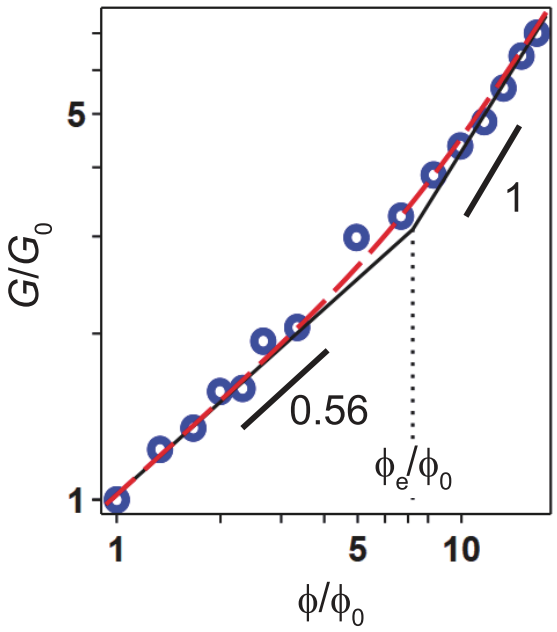

Figure 11: Dependence of the elastic modulus $G(\phi)$ of a deswollen network on polymer volume fractions ϕ. The network was prepared at the polymer volume fraction $\phi_0 = 0.91\phi^*$ (the overlap polymer volume fraction is estimated as $\phi^* = 0.07$ by using the Daoud-Cotton theory[25] for the 4-arm star polymers composed of 200 beads in an athermal solvent). The points represent simulation data by Asai *et al.*,[24] which are fitted by eq. (24) with the crossover exponent $k = 5.0$. Solid lines show the limiting scaling dependences $G(\phi)$ in different regimes. The polymer volume fraction at the entanglement crossover is estimated to be $\phi_e = 0.46$ by fitting the simulation data with eq. (24).

4.2 Disentanglement crossover

The maximum extent of network swelling is limited by the volume fraction $\phi_{\rm eq}$ at equilibrium swelling. Thus, the equilibrium volume fraction of well-entangled networks is only on the order of one decade lower than preparation volume fraction $\phi_0/\phi_{\rm eq} \approx N_{\rm em}^{24/35} \sim 10$. The non-affine tube model (which is equivalent to the non-affine loopy tube model in the description of network swelling) predicts that the disentanglement crossover is rather broad and truncated by the equilibrium swelling.[27] A much wider region of the disentanglement crossover can be explored by chemically attaching dangling polyelectrolytes to crosslinks in polymer networks. Dangling polyelectrolytes are elastically ineffective and do not contribute to the elastic energy of the network, while the osmotic pressure is increased by counterions entrapped by electrostatic interaction with dangling polyelectrolytes, as in the case of the molecular stent technique.[32]

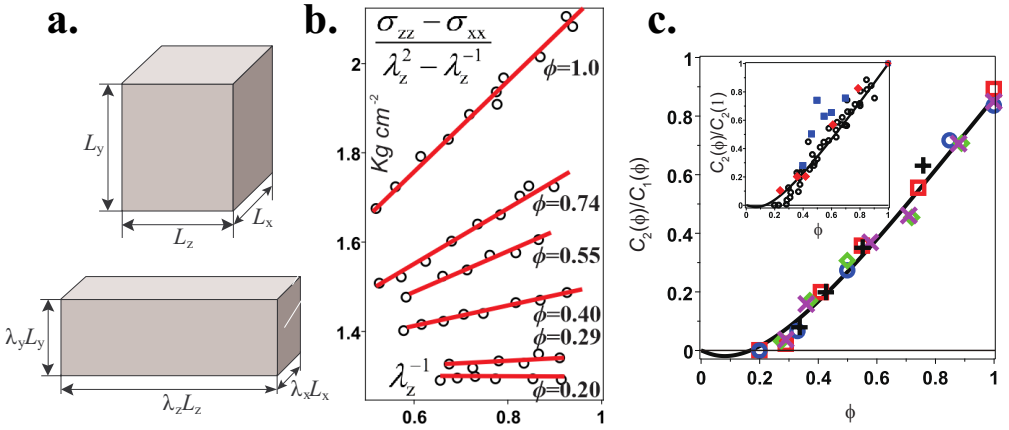

Figure 12: **a.** The uni-axial stretching of a polymer network by the stretching ratio λ_z in the z-axis. Because of the incompressibility of the system, the network is stretched by the stretching ratios λ_x and λ_y in the x- and y-axes, respectively. **b.** An example of the Mooney plot of the force-extension relationship of the polymer network (the data is extracted from ref.[28]). σ_{zz} is the normal stress in the z-axis and σ_{xx} is the normal stress in the x-axis. **c.** Dependence of the dimensionless ratio of Mooney-Rivlin constants $C_2(\phi)/C_1(\phi)$ on the polymer volume fraction ϕ. Solid lines were obtained using the non-affine tube model to describe a network prepared in melt ($\phi_0 = 1$).[27] Symbols show experimental data for rubbers[28] swollen in benzene (red squares), carbon tetrachloride (blue circles), petroleum ether 60/80 (purple $\times$), nitrobenzene (black +), decane (green diamonds). The inset shows the dependence of the dimensionless ratio $C_2(\phi)/C_2(1)$ on the polymer volume fraction ϕ. Experimental data are shown by the symbols: circles,[29] filled squares,[30] and filled diamond.[31]

The contribution of the trapped entanglements to the network elasticity can also be derived from the analysis of the force-extension relationships of polymer networks under the uni-axial deformation. Consider a network that was entangled at the preparation conditions, swollen in a θ-solvent to the polymer volume fraction ϕ and then uni-axially stretched in the z-direction by the extension ratio λ_z, see fig. 12**a**. On time scales shorter than the hydrostatic pressure relaxation time, the gel can be considered incompressible, $\lambda_x = \lambda_y = \lambda_z^{-1/2}$. Both the phantom and affine network models predict that the normal stress difference $\sigma_{zz} - \sigma_{xx}$ (where σ_{zz} and σ_{xx} are the normal stresses in z- and x-directions, respectively) is proportional to $\lambda_z^2 - \lambda_z^{-1}$. In the Mooney-Rivlin plot, the ratio of the normal stress difference to the factor $\lambda_z^2 - \lambda_z^{-1}$, plotted as a function of the inverse extension ratio λ_z^{-1}, highlights the deviation of the experimental results from predictions of the phantom and affine network models. The Mooney-Rivlin coefficients $C_1(\phi)$ and $C_2(\phi)$ are derived by fitting the data by the phenomenological equation[4]

$$\frac{\sigma_{zz} - \sigma_{xx}}{\lambda_z^2 - \lambda_z^{-1}} \simeq 2C_1(\phi) + \frac{2C_2(\phi)}{\lambda_z}, \tag{25}$$

see fig. 12**b**. The coefficient $C_2(\phi)$ is zero for phantom and affine network models and thus reflects the degree of the non-affine deformation of entangled networks.[4,26] The disentanglement of the network upon its swelling can be characterized by two dimensionless ratios of the Mooney-Rivlin coefficients $C_2(\phi)/C_1(\phi)$ and $C_2(\phi)/C_1(1)$. As seen from fig. 12**c**, these ratios decrease with decreasing polymer volume fraction ϕ and may vanish before gel reaches its equilibrium swelling. This means that even if the network has been entangled under the preparation conditions, the effect of crosslinks can dominate the effect of the trapped entanglements upon network swelling. Note that $C_2(\phi)$ vanishes upon swelling only for a rather narrow range of the parameter $N_{\rm x}/N_{\rm e0}$ in the diagram in Fig. 3, while in the case of $N_{\rm x} > N_{\rm e}^{\rm eq}$, $C_2(\phi)$ remains finite for any polymer volume fraction $\phi \geq \phi_{\rm eq}$.

4.3 Scaling exponents of the dependence of the elastic modulus on initial and final polymer volume fractions

The Flory-Rehner model[1] assumes that network strands are Gaussian and thus it describes well the unentangled networks in a θ-solvent. Although the Flory-Rehner model is also often used to describe the elasticity of networks in a good solvent, network strands in such networks are substantially non-Gaussian due to the excluded volume interactions between their monomers. Panyukov has developed an extended model (here we call it the *scaling model*) that takes into account the swelling of network strands in a good solvent, using the scaling theory.[10] Neither trapped nor transient entanglements are taken into account in this model. All the models of unentangled networks discussed in this paper are equivalent to the Flory-Rehner model for networks in a θ-solvent and the scaling model for networks in a good solvent, see the green filled circles in fig. 13 and also sec. 2.1 and 3.1.

Table 1: Scaling exponents κ_0 and κ of the dependence of the shear modulus, $G(\phi) \sim \phi_0^{\kappa_0}\phi^{\kappa}$, on the initial concentration ϕ_0 and the final concentration ϕ for polymer networks in good solvent for unentangled (U), entangled swollen (ES), and entangled deswollen (ED) regimes. The κ_0-exponent in the ED regime is given for networks unentangled at the preparation conditions (ED/U), and networks entangled at the preparation conditions (ED/E). 'Affine tube (S)' and 'Non-affine tube (S)' are extensions of the affine and non-affine tube models, taking into account intra-strand excluded volume interactions.

	κ_0				κ		
Model	U	ED/U	ED/E	ES	U	ES	ED
Non-affine loopy tube	0.44		1.3	1.53	0.56	0.78	1
Lattice animal[11]	0.44		1.2	1.98	0.56		1.1
Non-affine tube (S)[12]	0.44	1.1		1.53	0.56	0.78	1.2
Affine tube (S)[11]	0.44	-	1.98		0.56		
Scaling[10]	0.44	-	-	-	0.56	-	-

There are several approaches to describe the trapped and transient entanglements:

- *The affine tube model* takes into account the trapped entanglements by using the topological potential with the stiffness independent of network deformation, and assumes that neither additional trapped nor transient entanglements are produced upon network deswelling.[4,7] The predictions of the affine tube model for the dependence of the

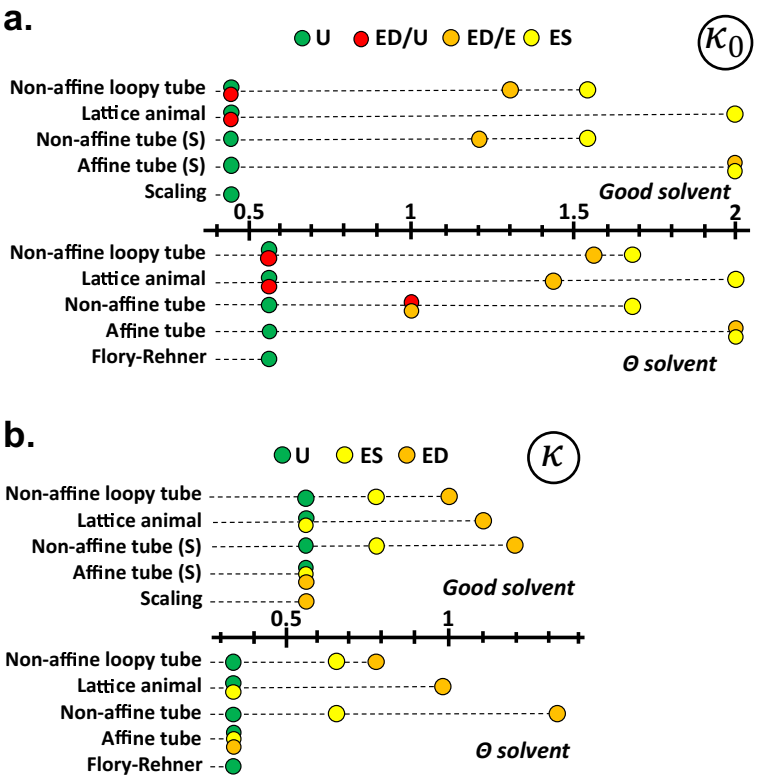

Figure 13: The scaling exponents κ_0 (**a**) and κ (**b**) of the dependence of the shear modulus, $G(\phi) \sim \phi_0^{\kappa_0}\phi^{\kappa}$, on initial polymer volume fraction ϕ_0 and final polymer volume fraction ϕ for polymer networks in an athermal solvent (upper) and θ-solvent (lower), see tables 1 and 2. Exponents for the unentangled ('U'), the entangled swollen ('ES'), and the entangled deswollen ('ED') regimes are shown by green, yellow, and orange filled circles, see also fig. 5 as well as tables 1 and 2. The κ_0 exponents depend on whether the networks were unentangled ('/U') or entangled ('/E') at the preparation conditions for the entangled deswollen regime, and are shown in red and orange filled circles, respectively.

Table 2: Scaling exponents, κ_0 and κ, of the dependence of the shear modulus, $G(\phi) \sim \phi_0^{\kappa_0}\phi^{\kappa}$, on the initial polymer volume fraction ϕ_0 and the final polymer volume fraction ϕ for polymer networks in a θ-solvent predicted by the non-affine loopy tube model and other models for unentangled (U), entangled swollen (ES), and entangled deswollen (ED) regimes. The κ_0-exponent at the ED regime is given for networks that were unentangled (ED/U) and entangled (ED/E) at the preparation conditions.

	κ_0				κ		
Model	U	ED/U	ED/E	ES	U	ES	ED
Non-affine loopy tube	2/3		14/9	5/3	1/3	2/3	7/9
Lattice animal[11]	2/3		10/7	2	1/3		19/21
Non-affine tube[12]	2/3	1		5/3	1/3	2/3	4/3
Affine tube[7,11]	2/3	-	2		1/3		
Flory-Rehner[1]	2/3	-	-	-	1/3	-	-

elastic modulus on the polymer volume fraction ϕ in the entangled regimes are the same as in the unentangled regime, see fig. 13 and tables 1 and 2.

- *The lattice animal model* is equivalent to the affine tube model in describing the trapped entanglements in swollen entangled networks and suggests that network strands of deswollen networks fold into the lattice animal conformations due to transient entanglements,[11] which corresponds to the conformations of entangled rings in the array of fixed obstacles[15,16]

- *The non-affine tube model* takes into account the dependence of the stiffness of the topological potential on the network deformation and is equivalent to the non-affine loopy tube model in the treatment of the trapped entanglements in swollen entangled networks.[12] In this model, it is assumed that the conformations of entanglement strands are Gaussian on the length scales between the correlation length ξ and the tube diameter a for both swollen and deswollen networks.

The elastic modulus predicted by the non-affine tube and non-affine loopy tube model decreases stronger upon the network swelling than the elastic modulus predicted by the affine tube model and the lattice animal model. This stronger decrease is due to the softening of the topological potential predicted by the non-affine tube and non-affine loopy tube models and is caused by the increasing distance between network strands upon gel swelling. The difference in the κ exponent between the two classes of models is more noticeable in the θ-solvent than in the good solvent conditions, see yellow circles in fig. 13 and tables 1 and 2. This difference can be experimentally measured and can serve as a criterion for the applicability of different models, because the exponent κ predicted by the non-affine loopy tube and non-affine tube models is twice as large as that predicted by the affine tube and lattice animal models. The exponent κ_0 predicted by the non-affine loopy tube and non-affine tube models also differs from the case of the affine tube and lattice animal models due to the dependence of the topological potential on the swelling ratio λ ($= (\phi_0/\phi)^{1/3}$), but the

difference is smaller, see yellow circles in fig. 13**b** and tables 1 and 2.

The non-affine loopy tube, non-affine tube, and lattice animal models predict that networks that were unentangled at preparation conditions become entangled upon network deswelling, while the affine tube model does not predict such a crossover. The non-affine loopy tube and lattice animal models assume that entanglements produced upon network deswelling are transient, whereas the non-affine tube model assumes that additional trapped entanglements are produced by network deswelling. Due to the creation of trapped entanglements, the exponent κ_0 predicted by the non-affine tube model is 2.5 times larger in the entangled deswollen regime than in the unentangled regime under the good solvent condition, see fig. 13**b** and table 1. In contrast to trapped entanglements, transient entanglements are not fixed by crosslinking during the preparation of the network, and the fluctuations of network strands, constrained by the transient entanglements, are determined solely by the number of overlapping strands at the final conditions. Thus, the exponent κ_0 predicted by these models is the same in the unentangled and entangled deswollen regimes if the networks were unentangled at preparation conditions, see also the discussion in the last paragraph of sec. 3.3.

In the entangled deswollen regime, the exponent κ_0 predicted by the non-affine tube model is independent of whether the networks were unentangled or entangled at preparation conditions, because the effect of these additional trapped entanglements produced by network deswelling dominates over the effects of the entanglements formed at preparation conditions and crosslinks. In contrast to the effect of trapped entanglements accounted for in the non-affine tube model, the transient entanglements predicted for a good solvent by the non-affine loopy tube model (and the lattice animal model) result in a scaling exponent κ_0, which is 3.0 times (and 2.7 times) larger for networks that were entangled at preparation conditions, compared to networks that were unentangled at these conditions, see red and orange circles in fig. 13b and table 1. The difference in the scaling exponent κ_0 between networks that were unentangled and entangled at preparation conditions reflects the fact

that the entanglements produced by network deswelling are transient in the non-affine loopy tube and lattice animal models: potential due to crosslinks (for the networks that were unentangled at the preparation condition) or topological potential (for the networks that were entangled at the preparation condition) still restricts fluctuations of strands in networks in entangled deswollen regime, see figs. 8 and 10. These features of transient entanglements versus trapped entanglements can be observed by measuring the dependence of the elastic modulus on the polymer volume fraction ϕ_0 at preparation conditions.

The non-affine loopy tube model predicts that the exponent κ to be unity in entangled deswollen regime under good solvent condition, see the top orange circle in fig. 13**a** and table 1. This prediction is consistent with simulations and experiments on tetra-PEG gels.[22–24] In entangled deswollen regime in a good solvent, the exponent κ predicted by the non-affine loopy tube model is 1.8 times greater than that predicted by the affine tube model, while the difference in the exponent κ between the non-affine loopy tube, non-affine tube, and lattice animal models is only 10 - 20 %, see orange circles in fig. 13**a** and table 1. The 60 % difference in the exponent κ between the non-affine tube and non-affine loopy tube models in the deswollen entangled regime in a θ solvent makes it possible to check which model is closer to simulations and experiments, see the corresponding orange circles in fig. 13 and table 2. It will be more difficult to separate the two transient entanglement models and to experimentally test whether the strands in deswollen networks adopt the fractal loopy globlue or lattice animal conformations, since the predictions of these models for the exponent κ in the entangled deswollen regime are within 16 % in a θ-solvent. It may be necessary to investigate the strand conformations directly, either by simulations or by scattering experiments.

4.4 Uniaxial extension of entangled deswollen networks

The network and entanglement strands form fractal loopy globule in the entangled deswollen regime. In secs. 3.2 and 3.3, we derived the elastic modulus of networks in this regime. At the

next step, it is of interest to theoretically predict the stress-strain relationship of deswollen entangled networks under uniaxial (and biaxial) extension. The number of monomers $N_{\rm aff}$ in the affine strands of the network that was unentangled in the preparation condition does not change upon deformation, see sec. 3.3. Network strands are extended like entangled rings in non-linear flows of solutions or melts:[35,36] tension blobs are developed in network strands under uniaxial extension. Network sections composed of n monomers form fractal loopy globules on scales larger than tension blobs for $g_{\rm t} < n < N_{\rm x}$ due to transient entanglements.

The maximal extension of strands in the network deswollen to the polymer volume fraction ϕ, is estimated as[11]

$$\lambda_{\rm max} \approx \left(\frac{\phi}{\phi_0}\right)^{1/3} \frac{bN_{\rm aff}}{\mathcal{R}_0(N_{\rm aff})}, \tag{26}$$

where $N_{\rm aff}$ is the number of monomers in the affine strand oriented in the stretching direction. $N_{\rm aff} = N_{\rm x}$ for a network that was unentangled in the preparation condition. Urayama and Kojiya determined the maximal extensibility of an end-linked PDMS network prepared from the precursor chains of the molecular weight 9.9×10^4 g/mol in a good solvent with polymer volume fraction 0.1.[38] By using eq. (26), the maximal extensibility $\lambda_{\rm max}$ of the network is estimated to be 27, which is consistent with the experimentally determined value of 25.[11]

The number of monomers $N_{\rm aff}$ in the affine strands of a network that was entangled in the preparation condition depends on the network deformation, because trapped entanglements can slide along the chains. The distribution of trapped entanglements, and thus the number of monomers $N_{\rm aff}$ in affine strands, is determined by the competition between the elasticity of the entanglement strands and the entropy of the trapped entanglements.[37] In ref.,[11] the maximal extensibility of networks deswollen to the dry state was estimated as $\lambda_{\rm max} \approx N_{\rm em}^{1/2}\phi_0^{-0.87}$ by assuming $N_{\rm aff} \approx N_{\rm e}(\phi_0)$, see eq. (26). However, in the general case, $N_{\rm aff}$ is a function of $\lambda_{\rm max}$ due to the redistribution of the trapped entanglements, and therefore, it is necessary to extend the non-affine loopy tube model in order to take into account

the sliding of trapped entanglements.

5 Conclusion

We have proposed and developed the non-affine loopy tube model that predicts the elasticity of swollen and deswollen networks. This theory takes into account three main mechanisms of elasticity of polymer networks: the crosslinks, trapped entanglements, and transient entanglements. Entanglements trapped at preparation conditions do not disappear with the subsequent deformation of the network but their effect decreases upon network swelling. Transient entanglements fold network strands into fractal loopy globules[17] and do not transmit elastic stress in the network over long time scales. The non-affine loopy tube model takes into account the fact that additional entanglements created upon network deswelling are not trapped, but are transient.

There are three regimes of the network elasticity: (i) Elasticity is mainly due to the crosslinks in the unentangled regime ('U' in figs. 5**a**), (ii) Elasticity dominated by the trapped entanglements in the entangled swollen regime ('ES' in figs. 5**a**), and (iii) Network strands are folded into fractal loopy globules due to the transient entanglements in the entangled deswollen regime ('DS' in figs. 5**a**). Under preparation conditions, networks are either unentangled at $N_{\rm x} < N_{\rm e0}$, or are entangled at $N_{\rm x} > N_{\rm e0}$. Networks that were entangled at preparation conditions at $N_{\rm e0} < N_{\rm x} < N_{\rm e}^{\rm eq}$ become unentangled upon network swelling. This disentanglement crossover occurs because the effect of trapped entanglements becomes weaker upon network swelling, as the neighboring chains move away from each other, while the effect of crosslinks is independent of the network deformation. Networks that were unentangled at preparation conditions at $N_{\rm em} < N_{\rm x} < N_{\rm e0}$ become entangled upon network deswelling. This entanglement crossover upon network deswelling occurs due to the transient entanglements produced as the neighboring chains approach each other upon network deswelling. The disentanglement crossover upon network swelling and the entangle-

ment crossover upon network deswelling can be observed experimentally by measuring the dependences of the network modulus on final concentration ϕ (see figs. 5**b**) as well as on the prepartion concentration ϕ_0 (see Fig. 7b). Transient entanglements also appear in networks that were entangled at preparation conditions upon network deswelling, and in this case the dependence of the elastic modulus on the polymer volume fraction ϕ changes at $\phi = \phi_0$.

Supporting Information Available

The Supporting Information ("TYMRsinglenetworkswellingver56revSI.pdf") are available free of charge: S1 Solvent conditions, S2 Networks deswollen in a θ-solvent, S3 Dry modulus, S4 Comparison with experiments.

Acknowledgement

This work was financially supported by the Institute for Chemical Reaction Design and Discovery (ICReDD), which has been established by the World Premier International Research Initiative (WPI), MEXT, Japan. M. R. acknowledges financial support from National Science Foundation, Center for the Chemistry of Molecularly Optimized Networks (CHE-2116298).

References

(1) Flory, P.J.; Rehner, J, Statistical Mechanics of Cross-Linked Polymer Networks I. Rubberlike Elasticity, *J. Chem. Phys.,* **1943,** *11,* 512-519.

(2) James, H.M.; Guth, E., Theory of the Elastic Properties of Rubber., *J. Chem. Phys.,* **1943,** *11,* 455-481.

(3) Treloar, L.R.G. *The physics of Rubber Elasticity.* Oxford University Press. NY, 1975.

(4) Rubinstein, M. and Colby, R., *Polymer Physics,* Oxford University Press, UK, 2003.

(5) de Gennes, P.G. *Scaling Concepts in Polymer Physics.* Cornell University Press, USA, 1979.

(6) Grest, G.S. and Kremer, K. Statistical Properties of Random Cross-Linked Rubbers. *Macromolecules*, **1990,** *23,* 4994-5000.

(7) Edwards S.F., The statistical mechanics of polymerized material. *Proc. Phys. Soc.,* **1967,** *92,* 9-16.

(8) Ball, R.C.; Doi, M.; Edwards, S.F.; Warner, M. Elasticity of entangled networks. *Polymers,* **1981,** *22,* 1010-1018.

(9) Edwards S.F.; Vilgis, Th. The effect of entanglements in rubber elasticity. *Polymers,* **1986,** *27,* 483-492.

(10) Panyukov, S.V. Scaling theory of high elasticity. *Sov. Phys. JETP,* **1990,** *71,* 372-379.

(11) Obukhov, S.P.; Rubinstein, M.; Colby, R.H., Network Modulus and Superelasticity. *Macromolecules* **1994,** *27,* 3191-3198.

(12) Rubinstein, M.; Panykov, S. Nonaffine Deformation and Elasticity of Polymer Networks. *Macromolecules* **1997,** *30,* 8036-8044.

(13) Panyukov, S.V., Topological interactions in the statistical theory of polymers, *Sov. Phys. JETP,* **1988**, *67*, 2274–2284.

(14) Panyukov, S.V., Topology fluctuations in polymer networks, *Sov. Phys. JETP*, **1989**, *69*, 342–353.

(15) Rubinstein, M. Dynamics of Ring Polymers in the Presence of Fixed Obstacles. *Phys. Rev. Lett.,* **1986,** *57,* 3023-3026.

(16) Obukhov, S.P.; Rubinstein M.; Duke, T. Dynamics of a Ring Polymer in a Gel. *Phys. Rev. Lett.,* **1994,** *73,* 1263-1266.

(17) Ge, T; Panyukov, S; Rubinstein, M. Self-Similar Conformations and Dynamics in Entangled Melts of Nonconcatenated Ring Polymers. *Macromolecules* **2016,** *49,* 708-722.

(18) Obukhov, S.; Johner, A.; Baschnagel, J.; Meyer H.; Wittmer J.P. Melt of polymer rings: The decorated loop model. *Europhys. Lett.* **2014,** *105,* 48005.

(19) Sariyer, O.S.; Panyukov, S.; Rubinstein, M. Nonlinear Elasticity of swollen gels. to be published.

(20) Kavassalis,T.A.; Noolandi,J. New view of Entanglements in Dense Polymer Systems. *Phys. Rev. Lett.,* **1987,** *59,* 2674-2677.

(21) Kavassalis,T.A.;Noolandi,J. A New Theory of Entanglements and Dynamics in Dense Polymer Systems. *Macromolecules,* **1988,** *21,* 2869-2879.

(22) Sakai T.; Kurakazu M.; Akagi Y.; Shibayama M.; Chung U.I. Effect of swelling and deswelling on the elasticity of polymer networks in the dilute to semi-dilute region. *Soft Matter,* **2012,** *8,* 2730-2736.

(23) Katashima T.; Asai M.; Urayama K.; Chung U.I.; Sakai T. Mechanical properties of tetra-PEG gels with supercoiled network structure. *J. Chem. Phys.* **2014,** *140,* 074902.

(24) Asai, M.; Katashima, T.; Sakai T.; Shibayama M. Supercoiling transformation of chemical gels. *Soft Matter,* **2015,** *11,* 7101-7108.

(25) Daoud, M.; Cotton,J.P. Star shaped polymers: a model for the conformation and its concentration dependence. *J. Phys.,* **1982,** 531.

(26) Wagner,M.H. The origin of the C_2 term in rubber elasticity. *J. Rheo.,* **1994,** *38,* 655-679.

(27) Panyukov, S. Theory of Flexible Polymer Networks: Elasticity and Heterogeneities. *Polymers,* **2020,** *12,* 767.

(28) Gumbrell, SM.; Mullins, L.; Rivlin, RS. Departures of the elastic behaviour of rubbers in simple extension from the kinetic theory. *Rubber Chem. Technol.,* **1955,** *28,* 24-35.

(29) Gumbrell, SM.; Mullins, L.; Rivlin, RS. Departures of the elastic behavior of rubbers in simple extension from the kinetic theory. *Trans. Faraday Soc.,* **1953,** *49,* 1495-1505.

(30) Ciferri, A.; Flory, PJ. Stress-Strain Isotherm for Polymer Networks. *J.* Appl. Phys., **1959,** *30,* 1498-1507.

(31) Allen, G.; Kirkham, MJ.; Padget J.; Price, C. Thermodynamics of Rubber Elasticity at Constant Volume. *1*971, **67,** *Trans. Faraday Soc.,* 1278-1292.

(32) Nakajima, T.; Sato, H.; Zhao, Y.; Kawahara, S.; Kurokawa, T.; Sugahara, K.; Gong, J.P. A Universal Molecular Stent Method to Toughen any Hydrogels Based on Double Network Concept. *Adv. Funct. Mater.,* **2012,** *22,* 4426-4432.

(33) Urayama, K.; Kohjiya, S. Uniaxial elongation of deswollen polydimethylsiloxane networks with supercoiled structure. *Polymer,* **1997,** *38,* 955-962.

(34) Vasiliev, V.G.; Rogovina L.Z.; Slonimsky, G.L. Dependence of properties of swollen and dry polymer networks on the conditions of their formation in solution. *Polymer,* **1985, 26,** 1667-1676.

(35) Huang, Q.; Ahn, J.; Parisi, D.; Chang, T.; Hassager, O.; Panyukov S.; Rubinstein M.; Vlassopoulos D. Unexpected Stretching of Entangled Ring Macromolecules. *Phys. Rev. Lett.,* **2019,** *122,* 208001.

(36) Parisi, D.; Costanzo, S; Jeong, Y.; Ahn, J.; Chang, T.; Vlassopoulos, D.; Halverson, J.D.; Kremer, K.; Ge, T.; Rubinstein, M.; Grest, G.S.; Srinin, W.; Grosberg, A.Y. Nonlinear Shear Rheology of Entangled Polymer Rings. *Macromolecules,* **2021,** *54,* 2811.

(37) Rubinstein, M.; Panykov, S. Elasticity of Polymer Networks. *Macromolecules* **2002,** *35,* s6670-6686.

(38) Urayama, K; Kohjiya, S. Extensive stretch of polysiloxane network chains with random- and super-coiled conformations. *Eur. Phys. J. B* **1998,** *2,* 75-78.

Graphical TOC Entry